



Experimental and numerical study on the effects of shaped multi-holes on the effectiveness of film cooling

Yaser Taheri¹ · Mehran Rajabi Zargarabadi¹ · Mehdi Jahromi²

Received: 24 January 2020 / Accepted: 4 August 2020 / Published online: 28 August 2020
© Akadémiai Kiadó, Budapest, Hungary 2020

Abstract

In the present work, experimental and numerical study has been performed to investigate the effects of a novel film-cooling design with shaped multi-holes on the film-cooling effectiveness over a flat plate. A single cylindrical hole with 11.1 mm diameter has been replaced by multi-holes (14 holes with 2.97 mm diameter) with elliptical and fan-shaped configurations. The exit area, length to diameter ratio ($L/D=4.0$) and injection angle (35°) of multi-holes are selected identical to the single cylindrical hole. The multi-holes were machined with a fixed spacing pitch (33.3 mm) between the centers of two adjacent holes. The surface temperature of the test plate was measured by an infrared camera. The experimental studies were performed at blowing ratios of 0.5 and 2. The numerical results based on the steady RANS with realizable $k-\epsilon$ turbulence model and enhanced wall treatment were capable to predict the influence of the shape of multi-hole configurations on overall adiabatic film-cooling effectiveness. The experimental and numerical results showed that replacing a single hole with a shaped multi-hole leads to a considerable increase in film-cooling effectiveness in both axial and lateral directions. According to the results at blowing ratio of 2.0, the elliptical and fan-shaped configurations provide a higher area-averaged film-cooling effectiveness by 75% and 248.2% in comparison with the single hole, respectively.

Keywords Experimental study · Film cooling · Multi-holes · Adiabatic effectiveness

Abbreviations

M	Blowing ratio $= (\rho U)_c / (\rho U)_\infty$
T	Temperature (K)
Tu	Turbulent intensity (%)
x/D	Non-dimensional streamwise distance
DR	Coolant to free-stream density ratio $= \rho_c / \rho_\infty$
D	Diameter of the hole (mm)
k	Turbulent kinetic energy ($\text{m}^2 \text{s}^{-2}$)
L	Length of the hole (mm)
Re	Reynolds number

η (eta)	Adiabatic film-cooling effectiveness; $\eta = \frac{T_{aw} - T_\infty}{T_j - T_\infty}$
ρ	Density of the fluid (kg m^{-3})
τ_w	Wall shear stress ($\text{kg m}^{-1} \text{s}^{-2}$)
μ	Dynamic viscosity ($\text{kg m}^{-1} \text{s}^{-1}$)
μ_t	Turbulent dynamic viscosity ($\text{kg m}^{-1} \text{s}^{-1}$)

Subscripts

j	Jet
∞	Free stream
aw	Adiabatic wall

Greek symbols

β	Streamwise injection angle ($^\circ$)
Θ	Internal energy (J)
θ	Heat flux (W m^{-2})
ϵ	Dissipation rate of turbulent kinetic energy ($\text{m}^2 \text{s}^{-3}$)

Introduction

One of the effective methods for enhancing the engine power and thermal efficiency of modern gas turbines is the increase of turbine inlet temperature, although, due to thermal stresses, this method may lead to the failure of high-temperature components. Hence, for the cooling of gas turbines external and internal cooling techniques are used. Among various techniques of cooling, film cooling is a common technique of external cooling which plays an important role for preventing the overheating of the hot section components. In film cooling, the air is ejected through the holes

✉ Mehran Rajabi Zargarabadi
rajabi@semnan.ac.ir

¹ Department of Mechanical Engineering, Semnan University, Semnan, Iran

² Malek Ashtar University of Technology, Tehran, Iran

in the desired surface to generate a layer of insulation over the plate. This layer of insulation protects the downstream surfaces of the holes from the hot gasses, which helps in maintaining the surfaces at the desired temperature.

The process of manufacturing a cylindrical hole is convenient, so these holes are widely used in film-cooling techniques. Many researches have been performed to investigate the effects of the geometrical parameters on cooling performance of the cylindrical holes [1–5]. Lutum and Johnson [2] evaluated the film-cooling effectiveness on a range of the hole length to diameter ratios between 1.75 and 18. They concluded that effectiveness decreases with decreasing the injection length when the L/D ratio was less than 5.0, but the change of effectiveness was not significant for $L/D > 5.0$. Experimental and numerical study on the effects of injection angle [3–5] highlighted that lower stream-wise injection angles can produce a higher film-cooling effectiveness.

Due to the jet lift-off and the undesirable effects of the counter-rotating vortex pair (CRVP) of cylindrical holes, shaped holes have been considered to improve the film-cooling effectiveness. Miao and Wu [6] and Leedom and Acharya [7] (by using cylindrical hole with 20 mm diameter) considered the use of a trench including cylindrical and forward-diffused holes. They found that the trenching diffused hole significantly improves the lateral spreading of the film-cooling effectiveness by weakening the CRVP at the hole exit. Gandhi and Suresh [8] studied the effect of mist concentration on the cooling effectiveness of hole with diffusion angle of 10° and 15° . Many studies considered the effects of different fan-shaped holds geometric factors on cooling performance [9–14]. Sun et al. [15] concluded that the shaped holes improve the film-cooling effectiveness through formation of a complex vortex structure which keeps the coolant jet attached to the wall.

The film-cooling performance of a converged-inlet shape with a cylindrical exit shape has been considered by Hee and Kwang [16]. They reported that applying a converged inlet on the cooling hole leads to an enhancement of the span-wise film-cooling effectiveness. Azzi and Jubran [17] (diameter was 12.7 mm) and Sargison et al. [18] (the cylindrical hole diameter was 20 mm) studied on convergent slot (console) geometry and found that the aerodynamic loss of console hole was reduced compared to a fan-shaped hole.

Although the shaped holes provide the higher film-cooling effectiveness compared to a common cylindrical hole, the shaped holes are difficult to make and expensive [19]. In recent years, the researchers developed new novel ideas to optimize the film-cooling effectiveness without using holes by shaped exits. Abdala and Elwekeel [20] used novel upstream steps with curved shapes to improve the film-cooling performance of a rectangular film hole ($D_h = 10$ mm). Lin Ye et al. [21] performed an experimental and numerical study to investigate the effects of inclined ribs on cooling

performance, Feng Zhang et al. [22]. The hydraulic diameter of holes in their study was 10 mm, and they reported the influence of upstream steps on the film-cooling effectiveness with unevenly spanwise distributed height.

Ely and Jubran [23] introduced a new design in film-cooling hole by applying the sister holes. Heidmann and Ekkad [24] presented anti-vortex holes to produce inverse vorticity versus the detrimental kidney vortices from standard circular film-cooling holes, which leads to better cooling performance. Dhungel et al. [25] and Leblanc et al. [26] considered the effects of orientations, geometry and pitch-to-diameter ratio of anti-vortex holes. Singh et al. [27] examined experimentally and numerically the effects of reverse injection cylindrical holes on creation of kidney vortices.

Reduction of the momentum of coolant injection is an effective way to weakened counter-rotating vortices, which achieved by employing a larger sectional zone at the hole exit, as the shaped holes. Under high blowing ratio, the shaped and novel ideas of film-cooling holes in comparison with the cylindrical holes have a better cooling performance, but the manufacturing cost of these holes is significantly higher [19]. Therefore, introducing a novel film-cooling designs using the common cylindrical holes can be worthwhile.

Although the effectiveness of film cooling can be improved by shaped holes, the manufacturing process of shaped hole can be very challenging in turbine blades. The present study introduces a novel fan-shaped film cooling by multi-cylindrical holes for increasing the film-cooling effectiveness. The flow structure and adiabatic cooling effectiveness of the multi-holes have been compared with a single cylindrical hole. Experimental and numerical results of the present study confirm that applying the multi-holes with shaped arrangement in comparison with a single cylindrical hole significantly increases the film-cooling effectiveness.

Experimental

Figure 1 shows a schematic sketch of the experimental setup. The mainstream air is supplied by a high-pressure centrifugal fan. In the secondary flow, an axial fan supplies the air which passes through a small tank. According to the figure, an electric heater is employed for heating the air which passes through a plenum. The secondary flow is controlled by a ball valve to adjust the desired velocity. The test section with $0.2 \text{ m} * 0.4 \text{ m}$ area is made up of Plexiglass material. As illustrated in Fig. 2, a row of multi-cylindrical holes with 2.97 mm diameter at the same inclination angle ($\alpha = 35^\circ$) and constant length to diameter ratio ($L/D = 4.0$) has been prepared. Every multi-holes consist of 14 cylindrical holes with a fixed spacing pitch of

Fig. 1 Schematic of the experiment setup

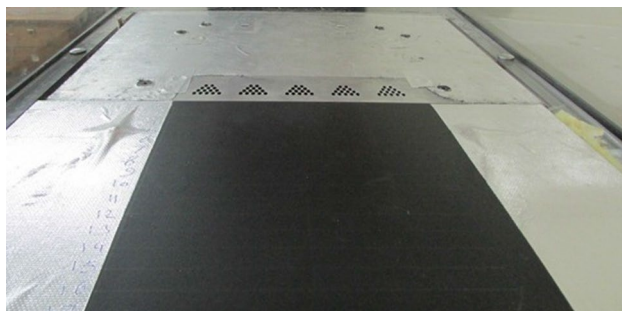
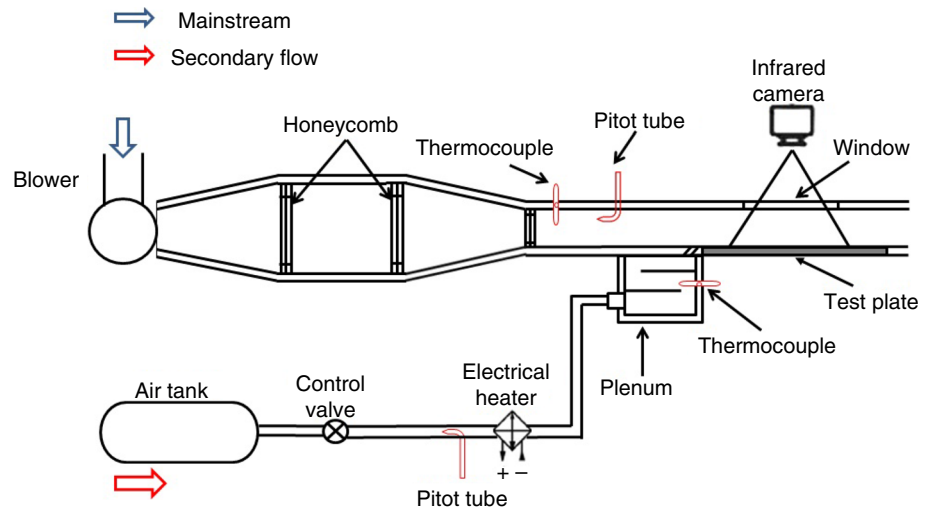


Fig. 2 A view of test surface

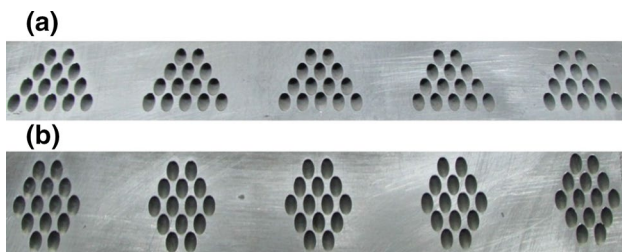


Fig. 3 Multi-holes configurations with **a** fan and **b** elliptical shaped

33.3 mm between centers of adjacent multi-holes. Multi-holes geometries with fan and elliptical shaped are tested (Fig. 3).

Figure 3 shows the fan-shaped and elliptical-shaped arrangements of the multi-holes. These holes were machined by milling on the aluminum plate. In order to achieve a uniform surface inside the holes, grinding has been performed with milling. This plate is assembled on top of the plenum. The bottom wall of the plate had been insulated with a thin glass-wool layer to reduce heat loss from the surface. Also all walls of the plenum were covered by a glass wool layers. The mainstream and secondary flow velocities were

Table 1 Uncertainties of measuring equipment

Equipment	Measuring errors
Infrared camera	$\pm (1.2 + 2.5\% \text{ rdg})$
K-type thermocouple	$\pm 0.4 T $
Pitot tube	$\pm 0.3\% F.S$
Power supply	$\pm 1.5\% F.S$

measured by calibrated Pitot tube located at a center of the stream.

The temperature of the secondary air is measured by a K-type thermocouple that is placed inside the plenum. There is a thermocouple upstream of the holes position to measure the mainstream flow temperature. The test plate used for these experimental setups is a stainless-steel sheet with 2 mm thickness which for minimizing the heat loss the back surface of the test plate is covered by glass wool insulation. The wall temperature distributions on the test plate have been measured by an infrared thermometer camera (EXTECH VIR50). The test plate is sprayed with identical black paint to provide a background for temperature measurement by an infrared thermometer camera. The calibration of the IR camera has been performed by a K-type thermocouple placed on the black-painted test surface to set up the emissivity of IR camera.

Analyzing the uncertainty of the experimental results in the present study can be estimated by identifying the main sources of the errors, such as uncertainty in keeping the velocity in constant value and setting the blowing ratio, accuracy of the temperature measuring instruments (K-type thermocouple and infrared camera) and accuracy of Pitot tube. Table 1 presents the measurement uncertainties of the directly measured parameters. Uncertainty has been done by the procedure proposed by Kline and McClintock [28]. The true value of the experimental data can be calculated

as the estimated value with its uncertainties multiplied by t distribution:

$$\mu = \bar{x} \pm S(\bar{x}) \cdot t_{\alpha/2}(n-1) \quad (1)$$

where $S(\bar{x})$ is variance of \bar{x} . The uncertainties of the cooling effectiveness can be determined with confidence of 95% (for $t_{\alpha/2}(n-1) = 2.78$). In the present study, the cooling effectiveness can be written as:

$$\eta = \eta(\bar{T}_w, \bar{T}_c, \bar{T}_h) \quad (2)$$

The measurements errors of experimental data are assumed to be independent. So the true value of η can be expressed as:

$$\eta_{\text{true}} = \eta \pm S(\bar{\eta}) \cdot t_{\alpha/2}(n-1) \quad (3)$$

The percent errors are calculated as:

$$\varepsilon_{\eta} = \frac{S(\bar{\eta}) \cdot t_{\alpha/2}(n-1)}{\eta} \quad (4)$$

Based on this methodology, the maximum computed uncertainty along the centerline of the holes was determined about 12%. In order to carry out better evaluation of multi-hole film cooling, numerical simulation is also performed

with consideration of test plate thickness and conduction heat transfer. So in numerical simulation, rather than adiabatic surface without thickness, test plate with stainless steel material and 2 mm thickness has been considered. The radiative losses can be neglected because the maximum temperature difference between the test plate and the mainstream flow is not significant and the emissivity coefficient of the test plate is very low ($e < 0.2$).

Numerical methodology

The computational domains in the present study include the plenum, film hole and mainstream duct. A single cylindrical hole with 11.1 mm diameter is utilized as the reference case for further comparisons with multi-cylindrical holes (see Fig. 4). The hole geometry has an injection angle and length to diameter ratio of 35° and 4.0, respectively. The plenum is 0.0508 m high and 0.1016 m length. As shown in Fig. 5, the computational domain of the multi-hole is obtained by replacing the area of the single cylindrical with 14 cylindrical holes with the same diameter of 2.97 mm. Multi-holes were arranged in elliptical- and fan-shaped configurations. These configurations are shown in Fig. 5. The center-to-center spacing of adjacent holes in these configurations was set to 1.5 D.

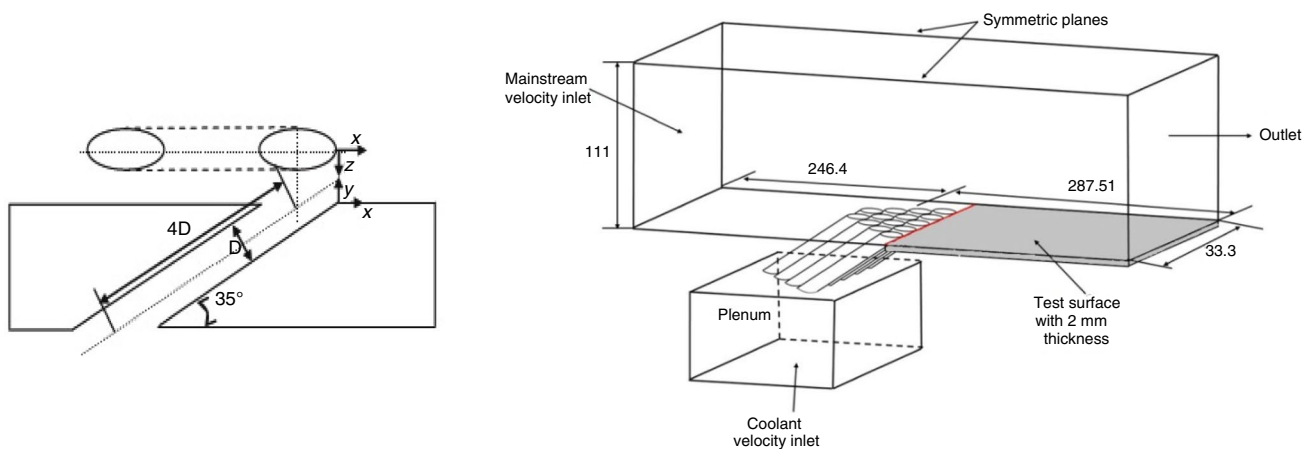
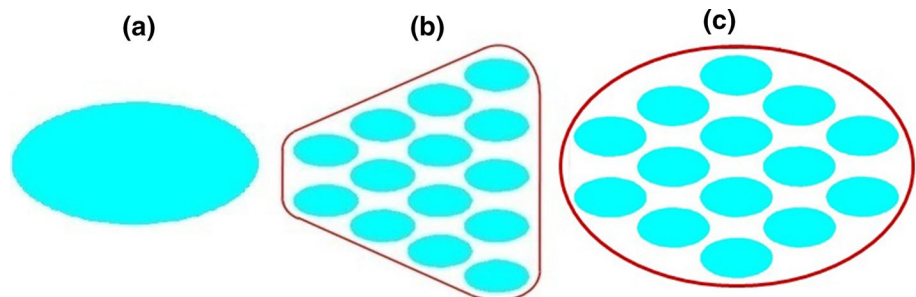


Fig. 4 Computational domain and boundary conditions (not drawn to scale)

Fig. 5 Film-cooling configurations **a** single hole, **b** fan-shaped multi-holes, **c** elliptical-shaped multi-holes



The Navier–Stokes equations have been solved by an element-based finite volume method with spatial discretization of the governing equations by using ANSYS FLUENT 16.0.0 [29].

$$\frac{\partial U_i}{\partial x_i} = 0 \tag{5}$$

$$\rho U_i \frac{\partial U_i}{\partial x_i} = -\frac{\partial p}{\partial x_j} + \mu \frac{\partial^2 \Theta}{\partial x_i \partial x_i} - \frac{\partial}{\partial x_i} (\rho \overline{u_i u_j}) \tag{6}$$

$$\rho \overline{u_i u_j} = \mu_t \left(\frac{\partial u_i}{\partial x_j} + \frac{\partial u_j}{\partial x_i} \right) - \frac{2}{3} \left(\rho k + \mu_t \frac{\partial u_k}{\partial x_k} \right) \delta_{ij} \tag{7}$$

$$U_i \frac{\partial \Theta}{\partial x_i} = \alpha \frac{\partial^2 \Theta}{\partial x_i \partial x_i} - \frac{\partial}{\partial x_i} (\overline{u_i \theta}) \tag{8}$$

In the present study the turbulent heat convection and the Reynolds stress are modeled with realizable *k*– ϵ model with enhanced wall treatment.

$$\frac{\partial}{\partial x_j} (\rho k u_j) = \frac{\partial}{\partial x_j} \left[\left(\mu + \frac{\mu_t}{\sigma_k} \right) \frac{\partial k}{\partial x_j} \right] + G_k + G_b - \rho \epsilon - Y_M + S_k \tag{9}$$

$$\begin{aligned} \frac{\partial}{\partial x_j} (\rho \epsilon u_j) &= \frac{\partial}{\partial x_j} \left[\left(\mu + \frac{\mu_t}{\sigma_\epsilon} \right) \frac{\partial \epsilon}{\partial x_j} \right] \\ &+ \rho C_1 S \epsilon - \rho C_2 \frac{\epsilon^2}{k + \sqrt{\nu \epsilon}} + C_{1\epsilon} \frac{\epsilon}{k} C_{3\epsilon} G_b + S_\epsilon \end{aligned} \tag{10}$$

μ_t is computed as a function of *k* and ϵ as follows:

$$\mu_t = \rho C_\mu \frac{k^2}{\epsilon} \tag{11}$$

where C_μ is not a constant. Details of the transport equations for the turbulence kinetic energy (*k*), and its dissipation rate (ϵ), the model constants and C_μ definition can be found in

Refs. [30, 31]. The pressure–velocity coupling algorithm is achieved by using the SIMPLEC algorithm. The residual error for convergence is set to 10^{-4} for continuity and 10^{-6} for momentum and for energy equations.

The multi-block structural meshes with hexagonal shaped and 1,686,100 cells were constructed and grid nodes considerably refined in the near-wall region to make sure that Y^+ values at the near wall cell are in the order of unity. Figure 6 shows the grids of these three blocks used for fan-shaped multi-holes. The domain over the flat plate is the first block, the coolant holes are the second, and the plenum is the third one. Also a Y^+ value at the near wall cell for fan-shaped multi-holes is shown in Fig. 7.

Symmetry boundary condition was used for the lateral planes in the main duct. The velocity inlet has been applied in the main stream and coolant air inlet. The out-flow boundary condition has been considered in the outlet condition.

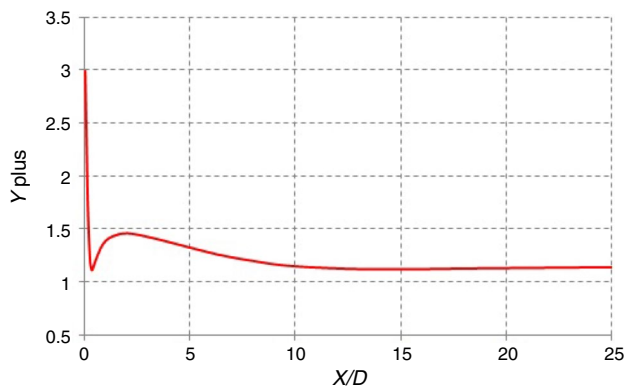
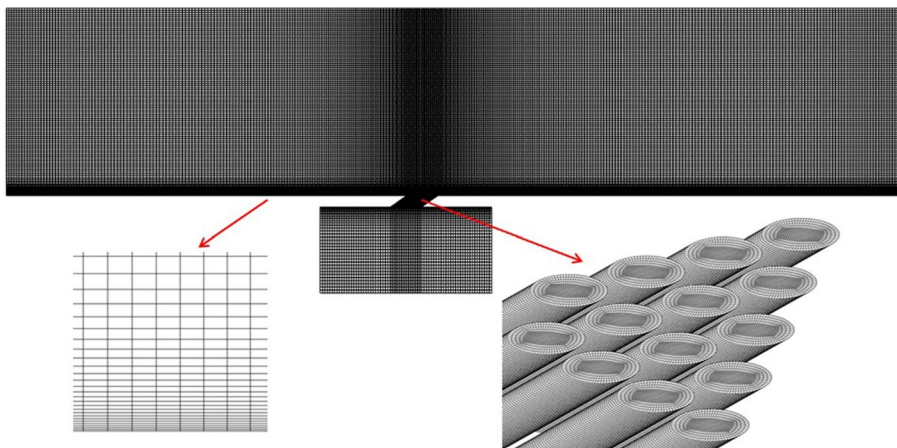


Fig. 7 Centerline Y^+ value for fan shaped multi-holes

Fig. 6 Computational grid for fan-shaped multi-holes



Validation of numerical simulation

In the present study the single-hole experimental results of Schmidt et al. [32] were selected for an accurate consideration of changes in the adiabatic performance of multi-holes. The uniform inlet velocity was set in the plenum inlet to achieve $Re = 18,700$, and the uniform mainstream duct velocity was adjusted to achieve the desired blowing ratio conditions. As given in Table 2, the operating parameters of the present study are identical to the experimental study of Schmidt et al. for validating the numerical solution. Numerical simulation was performed at blowing ratios 0.5, 1.25 and 2. Turbulence intensity of freestream and coolant is assumed 0.2 and 0.1%, respectively. The bottom surface of the mainstream duct, plenum and coolant hole was modeled as an adiabatic wall with no-slip condition. The grid independence for a single cylindrical hole is shown in Fig. 8.

Figure 9 compares the centerline adiabatic effectiveness of a single cylindrical hole with the experimental data of Schmidt et al. [32] at blowing ratios 0.6 and 1.25. The results show a good agreement with the experimental data, especially at near region of the hole. At high blowing ratio ($M = 1.25$) the coolant air lifts off from the surface which results in the film-cooling effectiveness decreases.

In this study, the film-cooling effectiveness of the multi-holes configuration is evaluated by both numerical and experimental studies. The results of the numerical simulation have been validated by the experimental data for further numerical studies. All geometric characteristics in the computation domain are identical to the experimental setup. In order to consider the conduction heat transfer, the stainless-steel sheet with 2 mm thickness has been also modeled in numerical simulation. A fully developed turbulent profile (1/7th law) with turbulence intensity of 10% was enforced at the mainstream inlet. According to the experimental conditions the mean temperature of mainstream and the hot flow (inside the plenum) are assumed to be 302.6 and 387.2 K, respectively. The experimental and numerical study (with test surface conduction) was performed at two blowing ratios 0.5 and 2.

The predicted centerline effectiveness is obtained by Eq. (12) as shown in Eq. (13) to estimate the lateral averaged effectiveness values. Numerical integration is used.

Table 2 Operating parameters of Schmidt et al. [32]

Property	Value
Freestream temperature	300 K
Blowing ratio	0.6 and 1.25
Density ratio	1.6
Coolant temperature	187.5 K

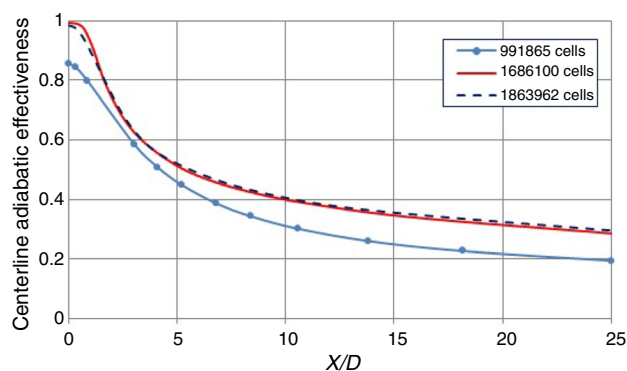


Fig. 8 Grid sensitivity for a single cylindrical hole, $M = 0.6$

$$\eta = \frac{T_{aw} - T_{\infty}}{T_C - T_{\infty}} \quad (12)$$

$$\bar{\eta} = \frac{1}{L} \int_0^L \eta dz \quad (13)$$

where L in Eq. (13) is the lateral distance between the symmetry boundaries.

Figures 10 and 11 compare the centerline film-cooling effectiveness of multi-holes arrangements obtained from the experimental and the present numerical studies. It can be seen that replacing a single cylindrical hole with multi-holes arrangement results to a considerable increase in film-cooling effectiveness.

Figure 10 shows that the numerical and experimental results are in good agreement with near and downstream of the hole. This is due to considering the wall thickness and modeling the conduction heat transfer through the wall. It is observed that conduction of heat transfer and the wall thickness of test surface has a significant effect on the

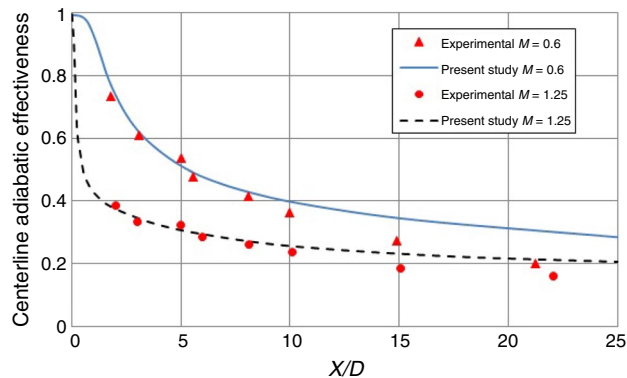


Fig. 9 Comparison of the centerline effectiveness of single hole with the experimental data [32]

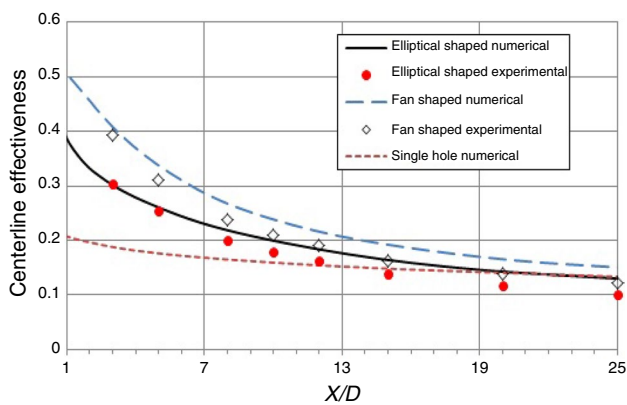


Fig. 10 Comparison of the centerline effectiveness of multi-holes with the experimental data at $M=0.5$

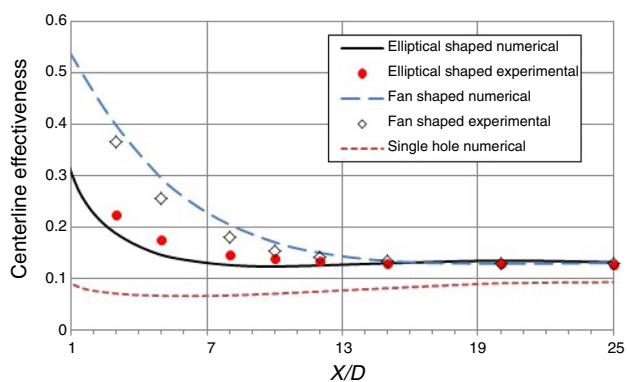


Fig. 11 Comparison of the centerline effectiveness of multi-holes with the experimental data at $M=2.0$

film-cooling effectiveness near the hole region [33, 34]. The experimental tests are performed to ensure the accuracy of numerical simulations, so it can be concluded that the

numerical simulation for single-hole and multi-holes configurations utilized in the present study is validated.

Results and discussion

The following section aims to represent the results of numerical simulations to explain the physical behavior of multi-holes arrangement. As mentioned in Table 2, the geometry and boundary conditions of the numerical study are identical to the experimental study of Schmidt et al. [32].

Figure 12 shows the temperature distributions on the centerline plane at blowing ratio of $M=2.0$. The cooling air and main stream interaction cause the formation of a counter-rotating vortices pair which consequences the coolant air to lift off from the surface. It can be seen in Fig. 12a that for single cylindrical a strong lift-off occurred that can be due to strong jet momentum and velocity gradient. As shown in Fig. 12b, c, for multi-holes configurations, the jet lift-off has been reduced, so the coolant remains in a close contact with the hot surface.

The velocity contours for cooling hole of a single and fan-shaped holes are displayed in Fig. 13. These contours are shown on the $x-y$ plane at $Z/D=0$. In the cooling hole, as the flow leaves the hole to the outlet, the flow velocity near the upper wall of the hole is increased, but for single cylindrical hole a large recirculating region appears on the lower wall and near the inlet of a hole.

Due to this jetting effect, at the upper exit of the hole, the coolant flow has locally high momentum [35]. Jetting effect increases the penetration of cooling fluid into the main stream, which results in separating of the cooling fluid from the surface and reducing the film-cooling effectiveness. However, according to Fig. 13b by applying the multi-holes configuration, the jetting effect is reduced, which causes the enhancement of the film-cooling effectiveness.

Fig. 12 Centerline plane temperature/K contours for $M=2.0$, **a** single hole, **b** elliptical-shaped holes, **c** fan-shaped holes

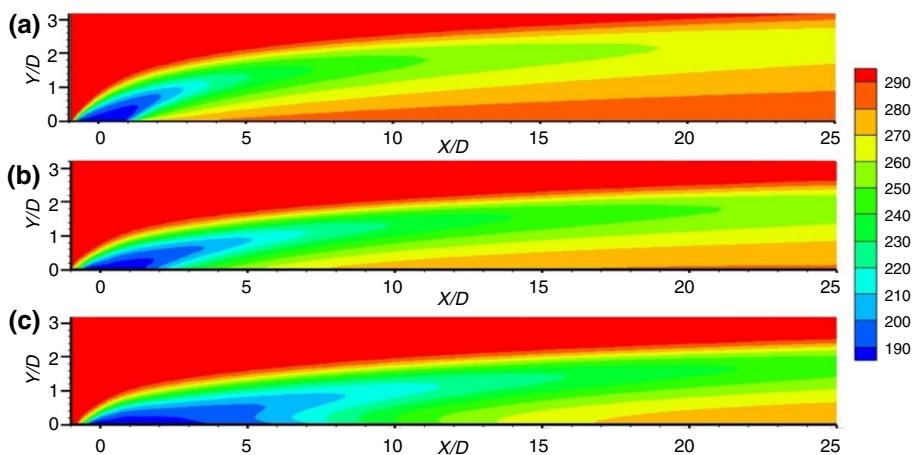


Figure 14 shows the streamwise (x) and vertical (y) velocity of cooling air near the jet exit for cylindrical hole and fan-shaped multi-holes. According to the figure, high velocity gradient can be observed for the cylindrical hole near the jet exit. The fan-shaped multi-holes configuration provides more uniform injected velocity. The high velocity gradient near the exit hole can produce high vorticity region. The vorticity exiting the film hole is the main contributing source for the counter-rotating vortices.

Figure 15 shows the velocity vectors at $X/D=3$ and temperature contours under the blowing ratio of $M=2.0$. The counter-rotating vortex pairs (CRVP) are the main reason of

reducing the film-cooling effectiveness. The CRVP are produced through the interaction between the main stream and the cooling flow [36, 37]. As shown in Fig. 15a the single cylindrical hole produces strong CRVP which pulls the hot mainstream inside the coolant air. However, by applying the multi-holes, these vortices are weakened and center of these vortices is generated lower than that for the single hole. For the fan-shaped multi-holes, the separated streams completely attach to the surface, thus spreading the low-temperature region on the surface. Also increasing the lateral distance and separating of kidney vortices reduces the strength of the vortex pairs [38, 39], which results in the cooling air

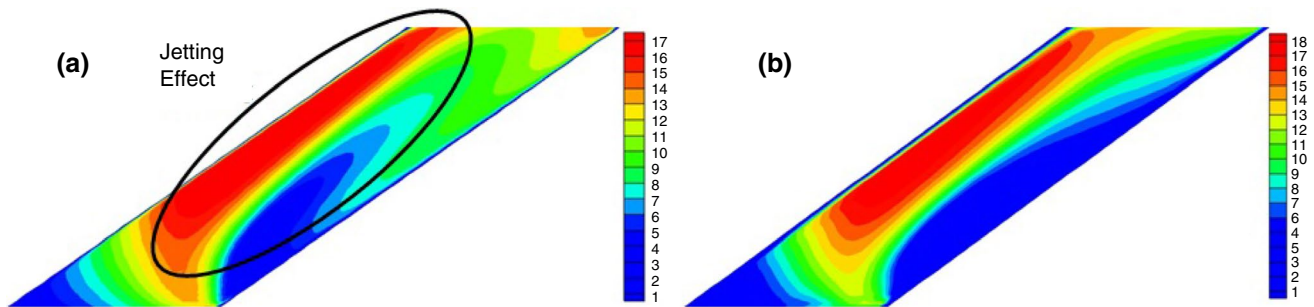


Fig. 13 Velocity/ $m\ s^{-1}$ contours at $z/D=0$ for **a** single hole, **b** multi-holes with fan shape

Fig. 14 Comparison of velocity contours (m/s) near the jet exit between cylindrical hole and fan-shaped multi-holes at $M=1.25$, **a** x velocity, **b** y velocity

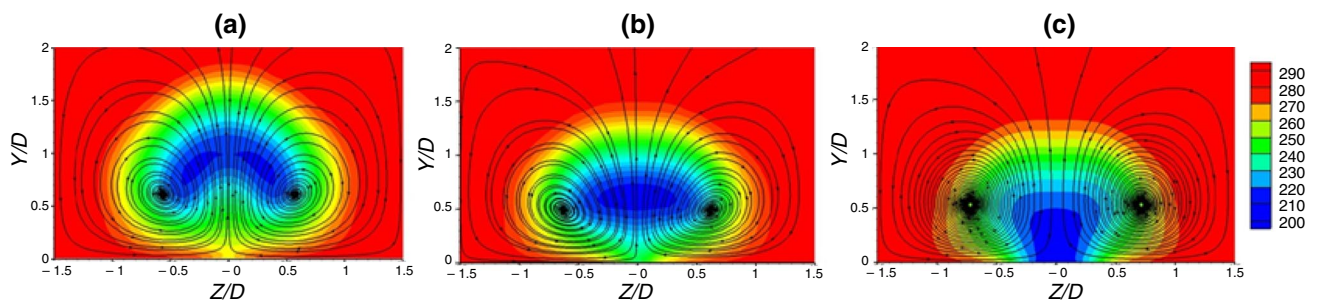
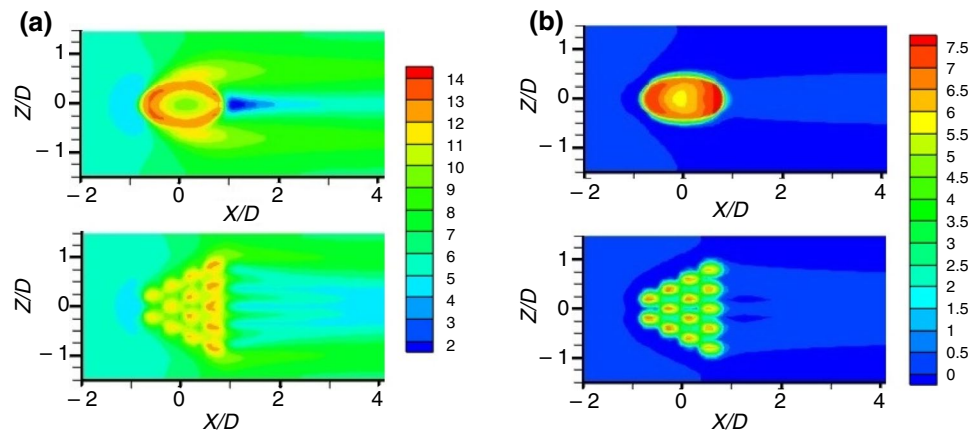
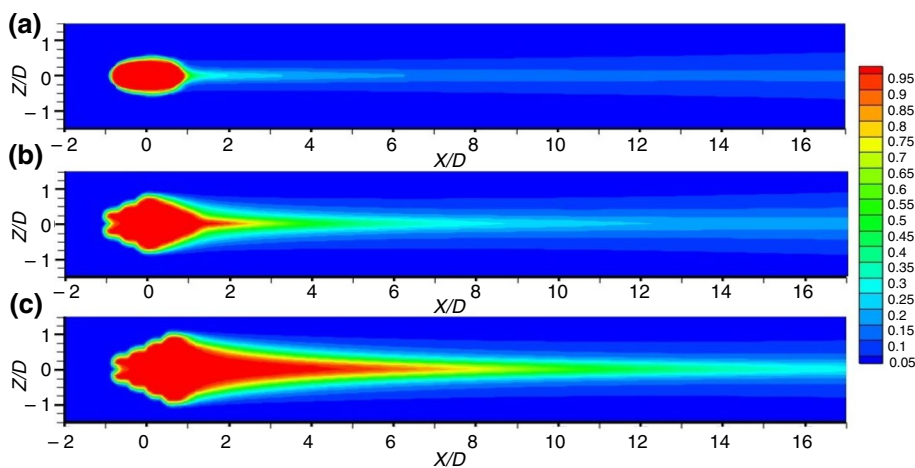


Fig. 15 Temperature/ K contours along with velocity/ $m\ s^{-1}$ vectors, $M=2.0$, $X/D=3$, **a** single hole, **b** elliptical-shaped holes, **c** fan-shaped holes

Fig. 16 Comparison the film-cooling effectiveness contours, $M=2$, **a** single hole, **b** elliptical-shaped holes, **c** fan-shaped holes



and tends to remain near the surface, and helps significantly enhance the film-cooling effectiveness, so that higher effectiveness is obtained.

The distribution of film-cooling effectiveness on the adiabatic wall at $M=2.0$ is represented in Fig. 16. As discussed in Figs. 13–15, due to the jet lift-off and mixing the coolant with hot mainstream, the values of cooling effectiveness in both streamwise and spanwise directions are very low for the single hole. When the multi-holes film cooling is used, the mixing of coolant and mainstream air is reduced and consequently the lateral and streamwise effectiveness is increased. It is notable that the configuration of multi-hole arrangement can significantly affect the distribution of the adiabatic film-cooling effectiveness.

The surface can be cooled for a longer-distance downstream of the cooling hole when using the multi-holes configuration. As shown in Fig. 16, the coverage of coolant for fan-shaped holes is better than elliptical-shaped holes in streamwise and spanwise directions.

The effects of blowing ratio on the film-cooling effectiveness in axial and spanwise directions are shown in Figs. 17 and 18. It can be observed that by increasing the blowing ratio from 0.5 to 2.0 the film-cooling effectiveness is reduced in both axial and spanwise directions. At high blowing ratio ($M=2.0$), the counter-rotating vortex pairs (CRVP) are placed farther from the surface because of increasing the vertical momentum of the coolant jet [40]. The streamwise vorticity in this case is dissipated less rapidly and are apparent much farther downstream. As illustrated in Fig. 15 by replacing the single hole with multi-holes the CRVP are moved near the wall.

When the multi-hole injection is used, the decrease in strength of kidney vortices and the mixing of coolant and mainstream, lead to a significant increase of the film-cooling effectiveness in comparison with single cylindrical hole. At higher blowing ratio, better cooling effectiveness in centerline can be obtained with fan-shaped multi-holes.

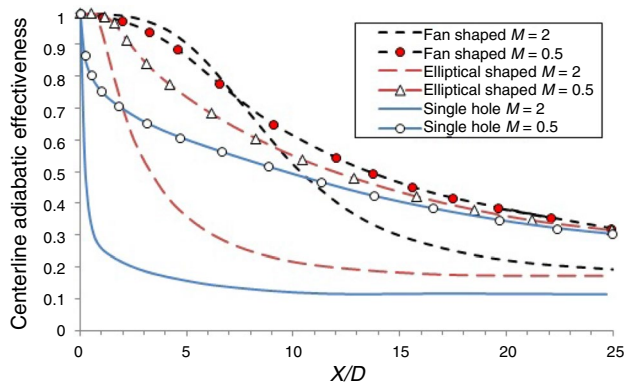


Fig. 17 Effects of blowing ratio on the centerline cooling effectiveness

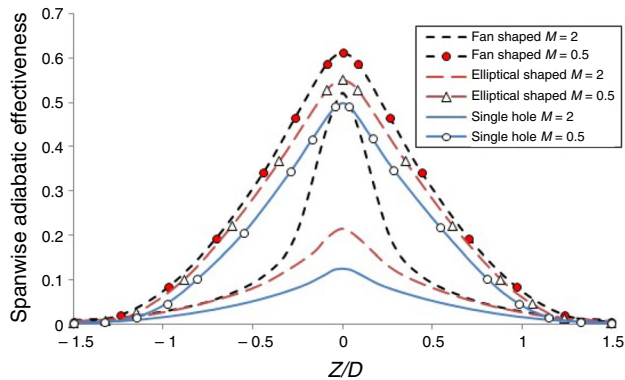


Fig. 18 Effects of blowing ratio on the spanwise cooling effectiveness ($X/D=10$)

Comparisons of the results show that under the blowing ratio of 2.0, the multi-holes arrangements provide much better coverage of effectiveness in both axial and spanwise directions. The centerline film-cooling effectiveness of

fan-shaped multi-holes shown in Fig. 17, is approximately three times that of the single cylindrical hole for $X/D < 15$.

The advantage of multi-hole arrangement can also be observed at spanwise direction. Figure 18 shows the effects of multi-hole configurations on the lateral effectiveness. It is clear that the fan-shaped multi-holes tend to provide the highest lateral effectiveness at both blowing ratios. As the blowing ratio increases from 0.5 to 2.0, more differences between lateral adiabatic effectiveness of fan shaped and single hole can be observed.

A comparison of the laterally averaged film-cooling effectiveness is presented in Fig. 19. It can be seen that the multi-holed arrangement provides much higher effectiveness at both blowing ratios of 0.5 and 2.0. With increasing blowing ratio, the differences of cooling effectiveness between the multi-holes and single cylindrical hole become more pronounced. Figure 18 indicates that the fan-shaped multi-hole provides superior film-cooling effectiveness at both blowing ratios ($M = 0.5, 2.0$) in comparison with single cylindrical hole and elliptical-shaped multi-holes.

The values of area-averaged film-cooling effectiveness for studied cases are reported in Table 3. In the present study the area-averaged film-cooling effectiveness is calculated by the following equation:

$$\bar{\eta}(x, z) = \frac{1}{3D * 15D} \int_{-1.5D}^{1.5D} \int_0^{15D} \eta(x, z) dx dz \quad (14)$$

According to Table 3, by decreasing the blowing ratio, area-averaged film-cooling effectiveness increases. The elliptical- and fan-shaped multi-holes provide a higher area-averaged film-cooling effectiveness by 42.7%, 130% more than the single cylindrical hole at blowing ratios of 1.25, respectively.

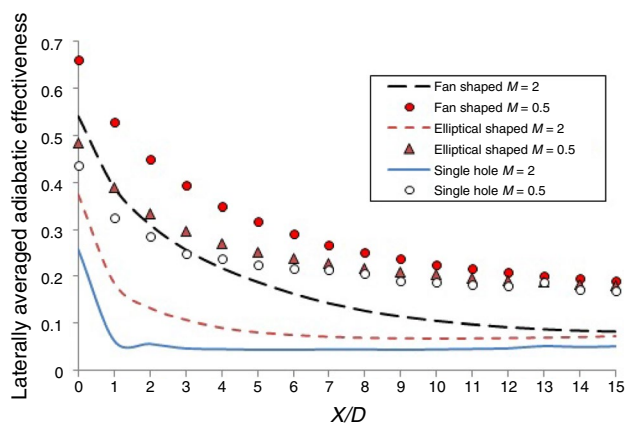


Fig. 19 Laterally averaged film-cooling effectiveness at $M = 0.5, 2$

Table 3 Comparisons of the area-averaged film-cooling effectiveness

Blowing ratio	Single hole	Elliptical shaped	Fan shaped
Area-averaged film-cooling effectiveness ($\bar{\eta}_{ave}$)			
$M = 0.5$	0.225	0.248	0.304
$M = 1.25$	0.110	0.157	0.253
$M = 2$	0.056	0.098	0.195

Conclusions

Numerical and experimental investigation is performed to enhance the cooling effectiveness over a flat plate by applying shaped multi-hole. A single cylindrical film-cooling hole with 11.1 mm diameter has been replaced with 14 small holes with 2.97 mm diameter. The multi-holes (14 small holes) have been arranged in two fan- and elliptical-shaped configurations. Numerical simulations are performed at length to diameter of 4, inclined angle of 35° and two blowing ratios of 0.6, 1.25 and 2. The steady RANS simulations with realizable $k-\epsilon$ turbulence model and enhanced wall treatment are conducted to validate the numerical simulation of the multi-holes arrangements. Since experimental test plate is not an adiabatic surface, numerical simulation with conduction boundary is also considered at blowing ratios 0.5 and 2.

The present study shows that the multi-hole configurations have a notable impact on the flow structure and heat transfer. The higher film effectiveness is achieved at low blowing ratio for single- and multi-holes configurations due to jets lift-off. Results of the present study indicate that the arrangement of multi-hole has a significant effect on the film-cooling effectiveness in both axial and lateral directions. The multi-holes generate weaker anti-vortices and jetting effect as compared with the single cylindrical hole which consequences a lower mixing between the hot main stream and the coolant air. It has been observed that replacing a single hole with the shaped multi-hole leads to a considerable increase in film-cooling effectiveness in both axial and lateral directions. The multi-hole with fan-shaped arrangement provides a better film protection in comparison with the single and elliptical-shaped configuration. It is found that the multi-hole with fan-shaped arrangement provides a higher area-averaged film-cooling effectiveness by 35.1%, 130% and 248.2% more than the single hole at blowing ratios of 0.5, 1.25 and 2, respectively.

References

- Hale CA, Plesniak MW, Ramadhyani S. Film cooling effectiveness for short film cooling holes fed by a narrow plenum. *J Turbomach.* 2000;122:553–7.
- Lutum E, Johnson BV. Influence of the hole length-to-diameter ratio on film cooling with cylindrical holes. *J Turbomach.* 1999;121:209–16.

3. Yuen CHN, Martinez-Botas RF. Film cooling characteristics of a single round hole at various streamwise angles in a crossflow: part I effectiveness. *Int J Heat Mass Transf.* 2003;46:221–35.
4. Nasir H, Ekkad SV, Acharya S. Effect of compound angle injection on flat surface film cooling with large streamwise injection angle. *Exp Therm Fluid Sci.* 2001;25:23–9.
5. Shine SR, Sunil Kumar S, Suresh BN. Internal wall-jet film cooling with compound angle cylindrical holes. *Energy Convers Manag.* 2013;68:54–62.
6. Miao JM, Wu CY. Numerical approach to hole shape effect on film cooling effectiveness over flat plate including internal impingement cooling chamber. *Int J Heat Mass Transf.* 2006;49:919–38.
7. Leedom DH, Acharya S. Large Eddy simulation of film cooling flow field from cylindrical and shaped holes. In: *ASME Turbo Expo 2008*, Paper No. GT2008–51009, June 9–13, Berlin, Germany.
8. Gandhi N, Suresh S. Effect of mist concentration on the cooling effectiveness of a diffused hole mist cooling system. *J Therm Anal Calorim.* 2020. <https://doi.org/10.1007/s10973-020-09680-1>.
9. Saumweber C, Schulz A. Effect of geometry variations on the cooling performance of fan-shaped cooling holes. In: *Proceedings of ASME Turbo Expo 2008*, GT2008–51038.
10. Gritsch M, Colban W, Schär H, Döbbling K. Effect of hole geometry on the thermal performance of fan-shaped film cooling holes. *J Turbomach.* 2005;127:718–25.
11. Peng W, Jiang PX. Experimental and numerical study of film cooling with internal coolant cross-flow effects. *Exp Heat Transf.* 2012;25:282–300.
12. Fua W-S, Chaoa W-S, Tsubokura M, Lic C-G, Wangd W-H. Investigation of boundary layer thickness and turbulence intensity on film cooling with a fan-shaped hole by direct numerical simulation. *Int Commun Heat Mass Transf.* 2018;96:12–9.
13. Lee KD, Kim KY. Shape optimization of a fan-shaped hole to enhance film cooling effectiveness. *Int J Heat Mass Transf.* 2010;53:2996–3005.
14. Fraas M, Glasenapp T, Schulz A, Bauer H-J. Optimized inlet geometry of a laidback fan-shaped film cooling hole—experimental study of film cooling performance. *Int J Heat Mass Transf.* 2019;128:980–90.
15. Sun X, Zhao G, Jiang P, Peng W, Wang J. Influence of hole geometry on film cooling effectiveness for a constant exit flow area. *Appl Therm Eng.* 2018;130:1404–15.
16. Kim J-H, Kim K-Y. Film-cooling performance of converged-inlet hole shapes. *Int J Therm Sci.* 2018;124:196–211.
17. Azzi A, Jubran BA. Numerical modelling of film cooling from converging slot-hole. *Heat Mass Transf.* 2007;43:381–8.
18. Sargison JE, Guo SM, Oldfield MLG, Lock GD, Rawlinson AJ. A converging slot-hole film cooling geometry—part 1: low-speed flat-plate heat transfer and loss. *J Turbomach.* 2002;124:453–60.
19. Chi Z, Ren J, Jiang H, Zang S. Geometrical optimization and experimental validation of a tripod film cooling hole with asymmetric side holes. *J Heat Transf.* 2016;138:061701.
20. Abdala AMM, Elwekeel FNM. An influence of novel upstream steps on film cooling performance. *Int J Heat Mass Transf.* 2016;93:86–96.
21. Ye L, Liu C-L, Liu H-Y, Zhu H-R, Luo J-X. Experimental and numerical study on the effects of rib orientation angle on film cooling performance of compound angle holes. *Int J Heat Mass Transf.* 2018;126:1099–112.
22. Zhang F, Wang X, Li J. The effects of upstream steps with unevenly spanwise distributed height on rectangular hole film cooling performance. *Int J Heat Mass Transf.* 2016;102:1209–21.
23. Ely MJ, Jubran BA. A numerical study on increasing film cooling effectiveness through the use of sister holes. *ASME Paper.* 2008; GT-50366.
24. Heidmann JD. A numerical study of anti-vortex film cooling designs at high blowing ratio. *ASME Paper.* 2008; GT-50845.
25. Dhungel A, Lu Y, Philips A, Ekkad S, Heidmann J. Film cooling from a row of holes supplemented with anti vortex holes. *ASME Paper.* 2007; GT2007–27419.
26. Leblanc C, Narzary D, Ekkad SV. Film cooling performance of an anti-vortex hole on a flat plate. *AJTEC2011–44161*, 2011 *AJTEC*, Hawaii, 2011.
27. Singh K, Premachandran B, Ravi MR. Experimental and numerical studies on film cooling with reverse/backward coolant injection. *Int J Therm Sci.* 2017;111:390–408.
28. Kline SJ, McClintock FA. Describing uncertainties in single-sample experiments. *Mech Eng.* 1953;75:3–8.
29. ANSYS Inc. ANSYS FLUENT 16.0.0, Cononsburg, PA, USA; 2014.
30. Shih T-H, Liou WW, Shabbir A, Yang Z, Zhu J. A new $k-\epsilon$ Eddy-viscosity model for high Reynolds number turbulent flows—model development and validation. *Comput Fluids.* 1995;24:227–38.
31. ANSYS Inc. ANSYS FLUENT theory guide, ANSYS FLUENT 16.0.0, Cononsburg, PA, USA; 2014.
32. Schmidt DL, Sen B, Bogard DG. Film cooling with compound angle holes: adiabatic effectiveness. *J Turbomach.* 1996;118(4):807–13.
33. Liu JH, Liu YB, Liu L. Film cooling modeling of a turbine vane with multiple configurations of holes. *Case Stud Therm Eng.* 2018;1:71–80.
34. Wang J, Gu C, Sundén B. Investigations of film cooling and its nonuniform distribution for the conjugate heat transfer passage with a compound inclined angle jet. *Numer Heat Trans Part A.* 2015;69:14–30.
35. Saumweber C, Schulz A. Effect of geometry variations on the cooling performance of fan-shaped cooling holes. In: *Proceedings of ASME Turbo Expo. 2008*; GT2008–51038.
36. Lylek JH, Zerkle RD. Discrete-jet film cooling: a comparison of computational results with experiments. *ASME J Turbomach.* 1994;113:358–68.
37. Moeini A, Zargarabadi MR. Genetic algorithm optimization of film cooling effectiveness over a rotating blade. *Int J Therm Sci.* 2018;125:248–55.
38. Haven BA, Kurosaka M. Kidney and anti-kidney vortices in cross-flow jets. *J Fluid Mech.* 1997;352:27–64.
39. Walters DK, Lylek JH. A detailed analysis of film-cooling physics: part I—streamwise injection with cylindrical holes. *ASME J Turbomach.* 2000;122:102–12.
40. Hyams DG, Lylek JH. A detailed analysis of film cooling physics: part 3—streamwise injection with shaped holes. *ASME J Turbomach.* 2000;122:122–32.

Publisher's Note Springer Nature remains neutral with regard to jurisdictional claims in published maps and institutional affiliations.